

# DEVELOPMENT OF A COMPUTER CODE FOR NEUTRONIC CALCULATIONS OF A HEXAGONAL LATTICE OF NUCLEAR REACTOR USING THE FLUX EXPANSION NODAL METHOD

by

**Meysam MOHAMMADNIA**<sup>1\*</sup>, **Ali PAZIRANDEH**<sup>1</sup>, and **Mostafa SEDIGHI**<sup>2</sup>

<sup>1</sup>Department of Nuclear Engineering, Science and Research Branch, Islamic Azad University, Tehran, Iran

<sup>2</sup>OCE, Ofogh Consulting Engineering Company, Tehran, Iran

Scientific paper

DOI: 10.2298/NTRP1303237M

The flux expansion nodal method is a suitable method for considering nodalization effects in node corners. In this paper we used this method to solve the intra-nodal flux analytically. Then, a computer code, named MA.CODE, was developed using the C# programming language. The code is capable of reactor core calculations for hexagonal geometries in two energy groups and three dimensions. The MA.CODE imports two group constants from the WIMS code and calculates the effective multiplication factor, thermal and fast neutron flux in three dimensions, power density, reactivity, and the power peaking factor of each fuel assembly. Some of the code's merits are low calculation time and a user friendly interface. MA.CODE results showed good agreement with IAEA benchmarks, *i. e.* AER-FCM-101 and AER-FCM-001.

*Key words:* flux expansion nodal method, hexagonal geometry, neutron flux distribution, MA.CODE

## INTRODUCTION

The reactor core is a heterogeneous medium with a limited size. When neutrons are distributed throughout the core, they may be absorbed by fuel, moderator, coolant, clad, and structural materials, or may leak out from the borders. The exact solution of core space equations is very important in the calculation of fuel burn-up and transient analysis. In order to convert the problem into a homogeneous medium, the core is usually divided into many areas.

A large number of approximation methods have been developed to enable a more computationally tractable solution for the effective multiplication constant and flux distribution in reactor cores. These methods can generally be classified as nodal, coarse-mesh, or synthesis methods [1].

Nodal methods characterize the global neutron flux distribution in terms of a small number of parameters in each of the several large regions, or nodes, into which the reactor core is subdivided for this purpose. Such methods generally require detailed heterogeneous intra-nodal flux distributions to construct homogenized parameters for each of the many nodes into which a reactor core may be divided and to calculate coupling parameters that link the average flux solution in adjacent nodes. Global average nodal fluxes must then be combined with the intra-nodal heterogeneous

flux solution if a heterogeneous flux distribution is required [1].

Conventional nodal methods are the first class of nodal models. The basis of such methods is the representation of the neutron flux or neutron fission rate within each of the many homogenized fuel assemblies by a single nodal average flux or fission rate that is coupled to the average flux or fission rate in adjacent nodes by the intra-nodal diffusion of the fast neutron which is represented by coupling coefficients [1].

The transverse integrated nodal method (TINM) is the second class of nodal methods. These methods have been formulated on the basis of integrating the 3-D diffusion equation over two transverse directions so as to obtain a 1-D diffusion equation, with transverse leakage terms, which can be solved within a node by approximating the dependence on the remaining spatial variable, usually with a polynomial. These methods are consistently formulated in that they reduce the limit of small node sizes to the conventional finite-difference method for the homogenized reactor model [1]. Among them, ANC-H [2, 3] and the analytical function expansion nodal (AFEN) method [4, 5] are most noticeable. They both eliminate the difficulties of performing transverse integration in hexagonal geometry and provide an accurate solution for various types of reactors. The ANC-H code converts hexagonal geometry into square geometry and squared relationships in the Cartesian system. In this method, due

\* Corresponding author; e-mail: m.mohamadnia@iauet.ac.ir



$$\psi_m(r) = \sum_{l=1}^6 [A_{ml}^\infty e^{\sqrt{\lambda_m} e_l r} + B_{ml}^\infty e^{-\sqrt{\lambda_m} e_l r}] \quad (11)$$

Eight interface partial currents and 10 first-order moments of the interface partial currents as the boundary conditions that constrain intra-nodal flux distributions in the hexagonal node are shown in fig. 1 [6].

Where arbitrary unit vectors are

$$\begin{aligned} e_\ell &= \cos \frac{(2\ell-3)\pi}{12} e_x + \sin \frac{(2\ell-3)\pi}{12} e_y, \ell = 1, 2, \dots, 6 \\ e_\ell &= e_z, \ell = 7 \\ e_\ell &= \cos \frac{\pi}{4} e_z + \sin \frac{\pi}{4} e_x, \ell = 8 \\ e_\ell &= \cos \frac{\pi}{4} e_z + \sin \frac{\pi}{4} e_y, \ell = 9 \end{aligned} \quad (12)$$

If  $\lambda_m = 0$ ,  $\sqrt{|\lambda_m|} = K_m$  and having  $e^x = \sinh x + \cosh x$  and  $e^{-x} = \cosh x - \sinh x$  eq. (11) by using arbitrary unit vectors of eq. (12) could be expanded into the following form

$$\begin{aligned} \psi_m(r) &= \sum_{\ell=1}^6 A_{m\ell} \sinh K_m x \cos \frac{(2\ell-3)\pi}{12} + y \sin \frac{(2\ell-3)\pi}{12} \\ &+ \sum_{\ell=1}^6 B_{m\ell} \cosh K_m x \cos \frac{(2\ell-3)\pi}{12} + y \sin \frac{(2\ell-3)\pi}{12} \\ &+ A_{m7} \sinh(K_m Z) + B_{m7} \cosh(K_m Z) \\ &+ A_{m8} \sinh K_m Z \cos \frac{\pi}{4} + x \sin \frac{\pi}{4} \\ &+ B_{m8} \cosh K_m Z \cos \frac{\pi}{4} + x \sin \frac{\pi}{4} \\ &+ A_{m9} \sinh K_m Z \cos \frac{\pi}{4} + y \sin \frac{\pi}{4} \\ &+ B_{m9} \cosh K_m Z \cos \frac{\pi}{4} + y \sin \frac{\pi}{4} \end{aligned} \quad (13)$$

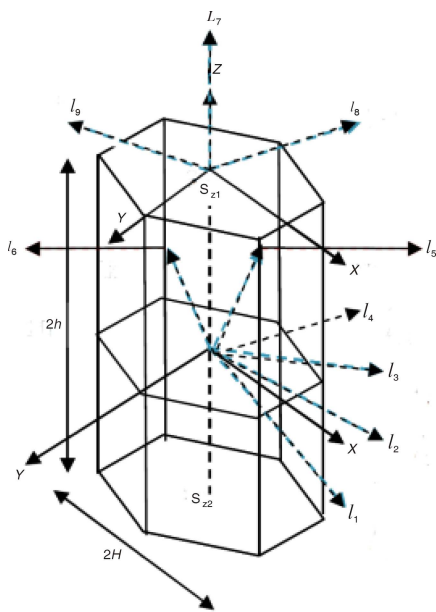


Figure 1. Co-ordinate system for the hexagonal node

If  $\lambda_m = 0$ ,  $\sqrt{|\lambda_m|} = iK_m$  and knowing that  $e^{ix} = \cos x + i \sin x$  and  $e^{-ix} = \cos x - i \sin x$ , eq. 11 by using arbitrary unit vectors of eq. 12 would be

$$\begin{aligned} \psi_m(r) &= \sum_{\ell=1}^6 A_{m\ell} \sin K_m x \cos \frac{(2\ell-3)\pi}{12} + y \sin \frac{(2\ell-3)\pi}{12} \\ &+ \sum_{\ell=1}^6 B_{m\ell} \sin K_m x \cos \frac{(2\ell-3)\pi}{12} + y \sin \frac{(2\ell-3)\pi}{12} \\ &+ A_{m7} \sin(K_m Z) + B_{m7} \cos(K_m Z) \\ &+ A_{m8} \sin K_m Z \cos \frac{\pi}{4} + x \sin \frac{\pi}{4} \\ &+ B_{m8} \cos K_m Z \cos \frac{\pi}{4} + x \sin \frac{\pi}{4} \\ &+ A_{m9} \sin K_m Z \cos \frac{\pi}{4} + y \sin \frac{\pi}{4} \\ &+ B_{m9} \cos K_m Z \cos \frac{\pi}{4} + y \sin \frac{\pi}{4} \end{aligned} \quad (14)$$

From eqs. (10) and (11) for the two groups of neutron energy in two modes, the following formula is obtained

$$\begin{aligned} \lambda_0 &= \frac{\Sigma_{d1}}{D_1} \frac{\nu \Sigma_{f1}}{k_{eff} D_1} - \frac{\nu_2 \Sigma_{f1}}{D_1} \\ &= \frac{\Sigma_{12}}{D_2} - \lambda_0 \frac{\Sigma_{12}}{D_2} \\ &= \sum_{\ell=1}^9 A_{0\ell} {}^1SN(K_0 e_\ell r) + \sum_{\ell=1}^9 B_{0\ell} {}^1CS(K_0 e_\ell r) \\ &= \sum_{\ell=1}^9 A_{0\ell} {}^2SN(K_0 e_\ell r) + \sum_{\ell=1}^9 B_{0\ell} {}^2CS(K_0 e_\ell r) \\ \lambda_1 &= \frac{\Sigma_{d1}}{D_1} \frac{\nu \Sigma_{f1}}{k_{eff} D_1} - \frac{\nu_2 \Sigma_{f2}}{D_1} \\ &= \frac{\Sigma_{12}}{D_2} - \lambda_0 \frac{\Sigma_{f2}}{D_2} \\ &= \sum_{\ell=1}^9 A_{1\ell} {}^1SN(K_1 e_\ell r) + \sum_{\ell=1}^9 B_{1\ell} {}^1CS(K_1 e_\ell r) = 0 \\ &= \sum_{\ell=1}^9 A_{1\ell} {}^2SN(K_1 e_\ell r) + \sum_{\ell=1}^9 B_{1\ell} {}^2CS(K_1 e_\ell r) = 0 \end{aligned} \quad (15)$$

The solution of eq. (15) leads to four sets of two equations in which four equations must be zero

$$\begin{aligned} A_{0\ell}^1 \frac{\Sigma_{12}}{D_2} - A_{0\ell}^2 \lambda_0 - \frac{\Sigma_{f2}}{D_2} &= 0 \\ A_{1\ell}^1 \frac{\Sigma_{12}}{D_2} - A_{1\ell}^2 \lambda_0 - \frac{\Sigma_{f2}}{D_2} &= 0 \\ B_{0\ell}^1 \frac{\Sigma_{12}}{D_2} - B_{0\ell}^2 \lambda_0 - \frac{\Sigma_{f2}}{D_2} &= 0 \\ B_{1\ell}^1 \frac{\Sigma_{12}}{D_2} - B_{1\ell}^2 \lambda_1 - \frac{\Sigma_{f2}}{D_2} &= 0 \end{aligned} \quad (16)$$

The solutions to eq. (16) are

$$\begin{matrix} S & \frac{A_{1\ell}^1}{A_{1\ell}^2} & \frac{B_{1\ell}^1}{B_{1\ell}^2} & \frac{D_2 \lambda_1}{12} & r_2 \\ R & \frac{A_{0\ell}^1}{A_{0\ell}^2} & \frac{B_{0\ell}^1}{B_{0\ell}^2} & \frac{D_2 \lambda_0}{12} & r_2 \end{matrix} \quad (17)$$

The relation between the auxiliary flux and the intra-nodal flux is

$$\begin{matrix} \varphi_1^-(X,Y,Z) & R & S \\ \varphi_2^-(X,Y,Z) & 1 & 1 \\ A_{0\ell} SN(K_0 e_\ell r) & B_{0\ell} CS(K_0 e_\ell r) \\ A_{1\ell} SN(K_1 e_\ell r) & B_{1\ell} CS(K_1 e_\ell r) \end{matrix} \quad (18)$$

In this equation, the intra-nodal flux is on the left and the second matrix on the right side of the equation is the auxiliary flux.

Eighteen unknown coefficients for  $A_{m\ell}$  and  $B_{m\ell}$  in two modes ( $m = 0, m = 1$ ) and two energy groups are obtained from the analytical integration of eq. (18). The boundaries of the surface integrals are introduced in fig. 2.

According to the integral boundaries, eq. (18) for surface number 1 and for modes 0 and 1 becomes

$$\begin{matrix} \bar{\varphi}_{g,1}^{r0} & \frac{1}{2h} \int_{-h}^h \frac{\sqrt{3}}{2H} \\ R & A_{0\ell} SN(K_0 e_\ell r) & B_{0\ell} CS(K_0 e_\ell r) \\ S & A_{1\ell} SN(K_1 e_\ell r) & B_{1\ell} CS(K_1 e_\ell r) \end{matrix} \Bigg|_{x=H} dy \quad (19)$$

$$\begin{matrix} \bar{\varphi}_{g,1}^{r1} & \frac{1}{2h} \int_{-h}^h (1) \frac{\sqrt{3}}{H} \\ R & A_{0\ell} SN(K_0 e_\ell r) & B_{0\ell} CS(K_0 e_\ell r) \\ S & A_{1\ell} SN(K_1 e_\ell r) & B_{1\ell} CS(K_1 e_\ell r) \end{matrix} \Bigg|_{x=H} dy + \frac{1}{2h} \int_{-h}^h (1) \frac{\sqrt{3}}{H} \\ R & A_{0\ell} SN(K_0 e_\ell r) & B_{0\ell} CS(K_0 e_\ell r) \\ S & A_{1\ell} SN(K_1 e_\ell r) & B_{1\ell} CS(K_1 e_\ell r) \end{matrix} \Bigg|_{x=H} dy \quad (20)$$

For the purpose of conciseness, correlations for surfaces 2-6 are not given here.

Coefficients for  $A_{m\ell}$  and  $B_{m\ell}$  from the above equations are defined by using new parameters named gamma factors. The said gamma factors are introduced in order to benefit from the symmetry of the hexagonal node. They are functions of  $K_m$  (buckling mode) and  $H$  (pitch).

$$\begin{matrix} k_m H \frac{2}{\sqrt{3}} \sin \frac{\pi}{4} Y_1, & k_m H \frac{2}{\sqrt{3}} \cos \frac{\pi}{12} Y_2 \\ k_m H \frac{2}{\sqrt{3}} \sin \frac{\pi}{12} Y_3, & k_m H \cos \frac{\pi}{4} Y_4 \end{matrix} \quad (21)$$

For mode 0, the aforementioned  $A_m$  and  $B_m$  coefficients are given in tab. 1.

For calculating  $\bar{\varphi}_{g,1}^{r0}$  when  $\lambda = (\lambda_0, \lambda_1)$  we have to add the results of multiplication of the first column by the second (third) column for each row. This is the case with other tables as well.

The average surface current for mode 0 and 1 for surface 1 can be written as

$$\bar{J}_{g,1}^{r0} = \frac{D_g}{2h} \int_{-h}^h \frac{\sqrt{3}}{2H} \frac{\partial \phi_g(x,y,z)}{\partial x} \Bigg|_{x=H} dy \quad (22)$$

Table 2 shows current coefficients for  $A_m$  and  $B_m$ .

$$\begin{matrix} \bar{J}_{g,1}^{r1} & \frac{D_g \sqrt{3}}{2H} \int_{-h}^h (1) \frac{\sqrt{3}}{2h} \frac{\partial \phi_g(x,y,z)}{\partial x} \Bigg|_{x=H} dy \\ \bar{J}_{g,1}^{r0} & \frac{D_g}{2h} \int_{-h}^h (1) \frac{\sqrt{3}}{2H} \frac{\partial \phi_g(x,y,z)}{\partial x} \Bigg|_{x=H} dy \end{matrix} \quad (23)$$

Correlations for the flux and current for the upper surface (+h) and the lower surface (-h) with their integral boundaries showed in figs. 1 and 2 are

$$\begin{matrix} \bar{\varphi}_{g,1}^{+0} & \frac{1}{2\sqrt{3}H^2} \\ R & A_{0\ell} SN(K_0 e_\ell r) & B_{0\ell} CS(K_0 e_\ell r) \\ S & A_{1\ell} SN(K_1 e_\ell r) & B_{1\ell} CS(K_1 e_\ell r) \end{matrix} \Bigg|_{z=+h} + \\ \begin{matrix} \bar{\varphi}_{g,1}^{-0} & \frac{1}{2\sqrt{3}H^2} \\ R & A_{0\ell} SN(K_0 e_\ell r) & B_{0\ell} CS(K_0 e_\ell r) \\ S & A_{1\ell} SN(K_1 e_\ell r) & B_{1\ell} CS(K_1 e_\ell r) \end{matrix} \Bigg|_{z=-h} \quad (24)$$

$$\begin{matrix} \bar{\varphi}_{1,1}^{+1} & \frac{1}{2\sqrt{3}H^2} \\ R & A_{0\ell} SN(K_0 e_\ell r) & B_{0\ell} CS(K_0 e_\ell r) \\ S & A_{1\ell} SN(K_1 e_\ell r) & B_{1\ell} CS(K_1 e_\ell r) \end{matrix} \Bigg|_{z=+h} + \\ \begin{matrix} \bar{\varphi}_{1,1}^{-1} & \frac{1}{2\sqrt{3}H^2} \\ R & A_{0\ell} SN(K_0 e_\ell r) & B_{0\ell} CS(K_0 e_\ell r) \\ S & A_{1\ell} SN(K_1 e_\ell r) & B_{1\ell} CS(K_1 e_\ell r) \end{matrix} \Bigg|_{z=-h} \quad (25)$$

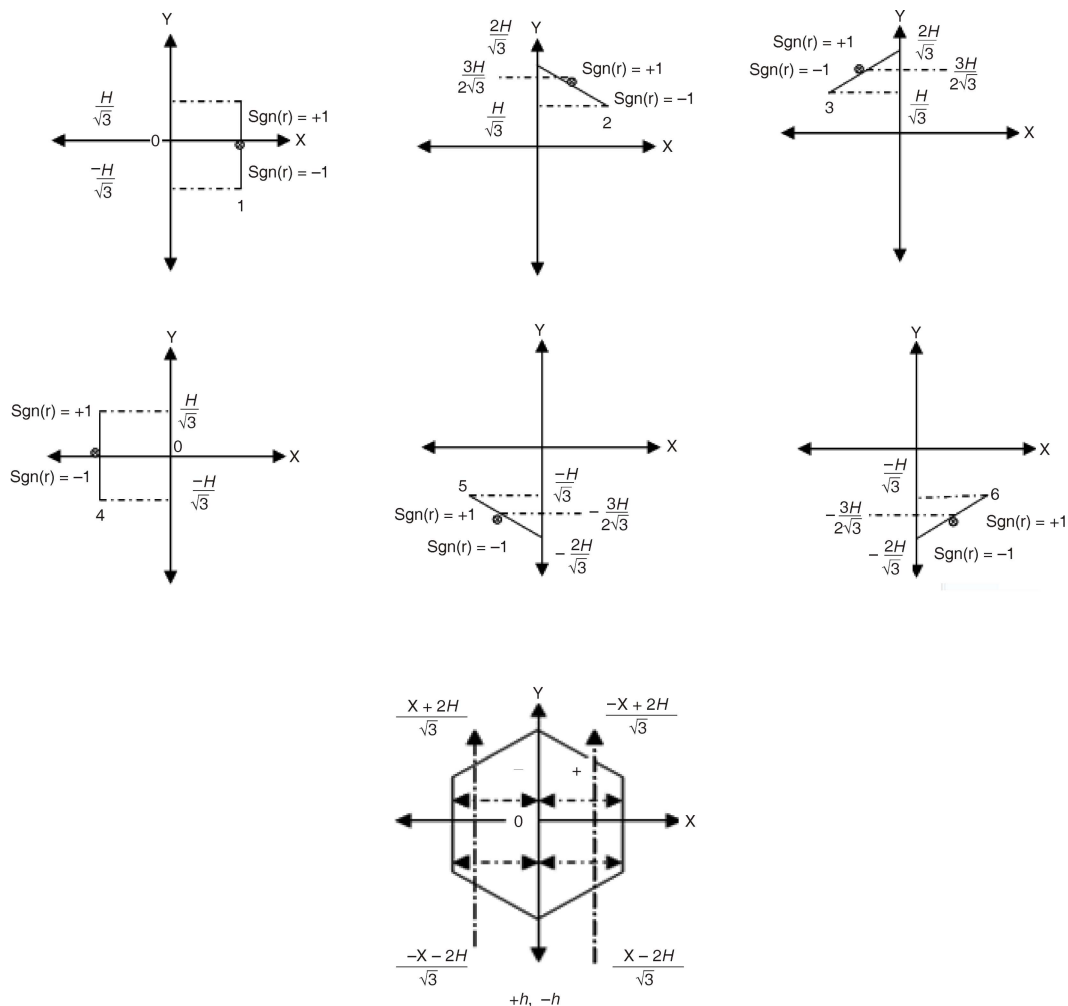


Figure 2. Integral boundaries of a hexagonal node

$$\begin{aligned}
 & \varphi_{1,1}^{zy,1} \frac{1}{2\sqrt{3}H^2} \\
 & \int_0^H dx \int_{\frac{x-2H}{\sqrt{3}}}^0 \left( R_{\ell 1}^9 A_{0\ell} SN(K_0 e_r) + B_{0\ell} CS(K_0 e_r) \right) \\
 & \quad S_{\ell 1}^9 A_{1\ell} SN(K_1 e_r) + B_{1\ell} CS(K_1 e_r) dy \Big|_{z_h} \\
 & + \int_0^H dx \int_0^{\frac{x-2H}{\sqrt{3}}} \left( R_{\ell 1}^9 A_{0\ell} SN(K_0 e_r) + B_{0\ell} CS(K_0 e_r) \right) \\
 & \quad S_{\ell 1}^9 A_{1\ell} SN(K_1 e_r) + B_{1\ell} CS(K_1 e_r) dy \Big|_{z_h} \\
 & + \int_H^0 dx \int_0^{\frac{x-2H}{\sqrt{3}}} \left( R_{\ell 1}^9 A_{0\ell} SN(K_0 e_r) + B_{0\ell} CS(K_0 e_r) \right) \\
 & \quad S_{\ell 1}^9 A_{1\ell} SN(K_1 e_r) + B_{1\ell} CS(K_1 e_r) dy \Big|_{z_h} \\
 & + \int_H^0 dx \int_{\frac{x-2H}{\sqrt{3}}}^0 \left( R_{\ell 1}^9 A_{0\ell} SN(K_0 e_r) + B_{0\ell} CS(K_0 e_r) \right) \\
 & \quad S_{\ell 1}^9 A_{1\ell} SN(K_1 e_r) + B_{1\ell} CS(K_1 e_r) dy \Big|_{z_h} \quad (26)
 \end{aligned}$$

$$\begin{aligned}
 \bar{J}_{g,1}^{z0} & \frac{D}{2\sqrt{3}H^2} \int_0^H dx \int_{\frac{x-2H}{\sqrt{3}}}^0 \frac{\partial \phi}{\partial z} dy \Big|_{z_h} \\
 & \int_H^0 dx \int_{\frac{x-2H}{\sqrt{3}}}^0 \frac{\partial \phi}{\partial z} dy \Big|_{z_h} \quad (27)
 \end{aligned}$$

$$\begin{aligned}
 \bar{J}_{g,1}^{z1} & \frac{D}{2\sqrt{3}H^2} \int_0^H dx \int_{\frac{x-2H}{\sqrt{3}}}^0 J_{g,k}^z dy \Big|_{z_h} \\
 & \int_H^0 dx \int_0^{\frac{x-2H}{\sqrt{3}}} J_{g,k}^z dy \Big|_{z_h} \quad (28)
 \end{aligned}$$

$$\begin{aligned}
 \bar{J}_{g,1}^{z1} & \frac{D_g}{2\sqrt{3}H^2} \int_0^H dx \int_{\frac{x-2H}{\sqrt{3}}}^0 J_{g,k}^z dy \Big|_{z_h} \\
 & \int_H^0 dx \int_0^{\frac{x-2H}{\sqrt{3}}} J_{g,k}^z dy \Big|_{z_h} \\
 & \int_H^0 dx \int_{\frac{x-2H}{\sqrt{3}}}^0 J_{g,k}^z dy \Big|_{z_h} + \int_0^H dx \int_0^{\frac{x-2H}{\sqrt{3}}} J_{g,k}^z dy \Big|_{z_h} \quad (29)
 \end{aligned}$$

**Table 1. Flux coefficients of first side ( $m = 0$ )**

	Coefficient when $\lambda_m > 0$	Coefficient when $\lambda_m < 0$
$A_{m1}$	$(Y_3)^{-1}(\cosh Y_1 - \cosh Y_2)$	$(Y_3)^{-1}(\cos Y_2 - \cos Y_1)$
$A_{m2}$	$(Y_3)^{-1}(\cosh Y_1 - \cosh Y_2)$	$(Y_3)^{-1}(\cos Y_2 - \cos Y_1)$
$A_{m3}$	$(Y_1)^{-1}2\sinh\sqrt{3}Y_l/2 \sinh Y_l/2$	$(Y_1)^{-1}2\sin\sqrt{3}Y_l/2 \sin Y_l/2$
$A_{m4}$	$(Y_2)^{-1}(\cosh Y_1 - \cosh Y_3)$	$(Y_2)^{-1}(\cos Y_3 - \cos Y_1)$
$A_{m5}$	$(Y_2)^{-1}(\cosh Y_3 - \cosh Y_1)$	$(Y_2)^{-1}(\cosh Y_3 - \cosh Y_1)$
$A_{m6}$	$(Y_1)^{-1}2\sinh\sqrt{3}Y_l/2 \sinh Y_l/2$	$(Y_1)^{-1}2\sin\sqrt{3}Y_l/2 \sin Y_l/2$
$A_{m7}, A_{m9}$	0	0
$A_{m8}$	$\sqrt{2}(k_m h)^{-1} \sinh Y_4 \sinh \sqrt{3}Y_l/2$	$\sqrt{2}(k_m h)^{-1} \sin Y_4 \sinh \sqrt{3}Y_l/2$
$B_{m1}$	$(Y_3)^{-1}(\sinh Y_1 - \sinh Y_2)$	$(Y_3)^{-1}(\sin Y_1 - \sin Y_2)$
$B_{m2}$	$(Y_3)^{-1}(\sinh Y_1 - \sinh Y_2)$	$(Y_3)^{-1}(\sin Y_1 - \sin Y_2)$
$B_{m3}$	$(Y_1)^{-1}2\cosh\sqrt{3}Y_l/2 \sinh Y_l/2$	$(\xi_1)^{-1}2\cos\sqrt{3}Y_l/2 \sin Y_l/2$
$B_{m4}$	$(Y_2)^{-1}(\sinh Y_1 - \sinh Y_3)$	$(Y_2)^{-1}(\sin Y_1 - \sin Y_3)$
$B_{m5}$	$(Y_2)^{-1}(\sinh Y_1 - \sinh Y_3)$	$(Y_2)^{-1}(\sin Y_1 - \sin Y_3)$
$B_{m6}$	$(Y_1)^{-1}2\cosh\sqrt{3}Y_l/2 \sinh Y_l/2$	$(Y_1)^{-1}2\cos\sqrt{3}Y_l/2 \sin Y_l/2$
$B_{m7}$	$(k_m h)^{-1} \sinh \sqrt{2}Y_4$	$(k_m h)^{-1} \sin \sqrt{2}Y_4$
$B_{m8}$	$\sqrt{2}(k_m h)^{-1} \sinh Y_4 \cosh \sqrt{3}Y_l$	$\sqrt{2}(k_m h)^{-1} \sin Y_4 \cos \sqrt{3}Y_l/2$
$B_{m9}$	$2\sqrt{3}(k_m^2 h H)^{-1} \sinh Y_4 \sinh Y_l/2$	$2\sqrt{3}(k_m^2 h H)^{-1} \sin Y_4 \sin Y_l/2$

**Table 2. Current coefficients of first side ( $m = 0$ )**

	$\lambda_m > 0$	$\lambda_m < 0$
$A_{m1}$	$k_m \cos \pi/12(Y_3)^{-1}(\sinh Y_1 - \sinh Y_2)$	$k_m \cos \pi/12(Y_3)^{-1}(\sin Y_1 - \sin Y_2)$
$A_{m2}$	$k_m \cos \pi/12(Y_3)^{-1}(\sinh Y_1 - \sinh Y_2)$	$k_m \cos \pi/12(Y_3)^{-1}(\sin Y_1 - \sin Y_2)$
$A_{m3}$	$k_m \cos \pi/4(Y_1)^{-1}2 \cosh \sqrt{3}Y_l/2 \sinh Y_l/2$	$k_m \cos \pi/4(Y_1)^{-1}2 \cos \sqrt{3}Y_l/2 \sin Y_l/2$
$A_{m4}$	$k_m \sin \pi/12(Y_2)^{-1}(\sinh Y_1 - \sinh Y_3)$	$k_m \sin \pi/12(Y_2)^{-1}(\sin Y_1 - \sin Y_3)$
$A_{m5}$	$k_m \sin \pi/12(Y_2)^{-1}(\sinh Y_1 - \sinh Y_3)$	$k_m \sin \pi/12(Y_2)^{-1}(\sin Y_1 - \sin Y_3)$
$A_{m6}$	$k_m \cos \pi/4(Y_1)^{-1}2 \cosh \sqrt{3}Y_l/2 \sinh Y_l/2$	$k_m \cos \pi/4(Y_1)^{-1}2 \cos \sqrt{3}Y_l/2 \sin Y_l/2$
$A_{m7}, A_{m9}$	0	0
$A_{m8}$	$h^{-1} \sinh Y_4 \cosh \sqrt{3}Y_l/2$	$h^{-1} \sin Y_4 \cos \sqrt{3}Y_l/2$
$B_{m1}$	$k_m \cos \pi/12(Y_3)^{-1}(\cosh Y_1 - \cosh Y_2)$	$k_m \cos \pi/12(Y_3)^{-1}(\cos Y_2 - \cos Y_1)$
$B_{m2}$	$k_m \cos \pi/12(Y_3)^{-1}(\cosh Y_1 - \cosh Y_2)$	$k_m \cos \pi/12(Y_3)^{-1}(\cos Y_2 - \cos Y_1)$
$B_{m3}$	$k_m \cos \pi/4(Y_1)^{-1}2 \sinh \sqrt{3}Y_l/2 \sinh Y_l/2$	$k_m \cos \pi/4(Y_1)^{-1}2 \sin \sqrt{3}Y_l/2 \sin Y_l/2$
$B_{m4}$	$k_m \sin \pi/12(Y_2)^{-1}(\cosh Y_1 - \cosh Y_3)$	$k_m \sin \pi/12(Y_2)^{-1}(\cos Y_3 - \cos Y_1)$
$B_{m5}$	$k_m \sin \pi/12(Y_2)^{-1}(\cosh Y_1 - \cosh Y_3)$	$k_m \sin \pi/12(Y_2)^{-1}(\cos Y_3 - \cos Y_1)$
$B_{m6}$	$k_m \cos \pi/4(Y_1)^{-1}2 \sinh \sqrt{3}Y_l/2 \sinh Y_l/2$	$k_m \cos \pi/4(Y_1)^{-1}2 \sin \sqrt{3}Y_l/2 \sin Y_l/2$
$B_{m7}, B_{m9}$	0	0
$B_{m8}$	$h^{-1} \sinh Y_4 \sinh \sqrt{3}Y_l/2$	$h^{-1} \sin Y_4 \sin \sqrt{3}Y_l/2$

Equation 30 shows the average partial current in the two modes and two groups of neutron energy for the six lateral surfaces of the hexagonal node, while eq. (31) is for the upper and lower surfaces.

$$\bar{J}_{g,k}^{r,\mu} = \frac{1}{4}\bar{\Phi}_{g,k}^{r,\mu} - \frac{1}{2}\bar{J}_{g,k}^{r,\mu}, \quad g = 1, 2, \mu = 0, 1, k = 1, 2, \dots, 6 \quad (30)$$

$$\bar{J}_{g,k}^{z,\mu} = \frac{1}{4}\bar{\Phi}_{g,k}^{z,\mu} - \frac{1}{2}\bar{J}_{g,k}^{z,\mu}, \quad g = 1, 2, \mu = 0, 1, k = 1, 2 \quad (31)$$

$\bar{J}$  and  $\bar{J}$  as the zero and first moment of the internal and external currents are defined in eqs. (32) and

(33) in which  $\bar{\Gamma}$  and  $\bar{\Gamma}$  are constant matrixes whose arrays depend on  $K_{eff}$  and node group diffusion.  $C$  is a matrix which defines intra-nodal flux coefficients

$$\bar{J} = \bar{\Gamma} C \quad (32)$$

$$\bar{J} = \bar{\Gamma} C \quad (33)$$

Matrix  $C$  is calculated in an iterative process between eqs. (32) and (33).  $\bar{J}$  in eq. (32) depends on external boundary conditions and external currents from neighboring nodes. We used the Gauss elimination

method to determine C in eq. (32). Then, by substituting matrix C in eq. (33), external partial currents were calculated. The external currents from the node are the internal currents of the neighboring nodes.

Finally, the volumetric average flux for the hexagonal node is obtained in eq. (34) by substituting the flux coefficients in the volumetric average flux correlation; the average neutron flux for each group and node is achieved in order to be used for the calculation of  $K_{eff}$  from the power-method.

$$\begin{aligned} \varphi_{total} &= (4\sqrt{3}H^2h)^{-1} \\ & \int_0^h \int_0^{\frac{x}{\sqrt{3}}} \int_0^{\frac{x}{\sqrt{3}}} R_{\ell 1}^9 A_{0\ell} SN(K_0 e_{\ell} r)_{\ell 1}^9 B_{0\ell} CS(K_0 e_{\ell} r)_{\ell 1}^9 \\ & S_{\ell 1}^9 A_{1\ell} SN(K_1 e_{\ell} r)_{\ell 1}^9 B_{1\ell} CS(K_1 e_{\ell} r)_{\ell 1}^9 dx dy dz \\ & + \int_0^h \int_0^{\frac{x}{\sqrt{3}}} \int_0^{\frac{x}{\sqrt{3}}} R_{\ell 1}^9 A_{0\ell} SN(K_0 e_{\ell} r)_{\ell 1}^9 B_{0\ell} CS(K_0 e_{\ell} r)_{\ell 1}^9 \\ & S_{\ell 1}^9 A_{1\ell} SN(K_1 e_{\ell} r)_{\ell 1}^9 B_{1\ell} CS(K_1 e_{\ell} r)_{\ell 1}^9 dx dy dz \quad (34) \end{aligned}$$

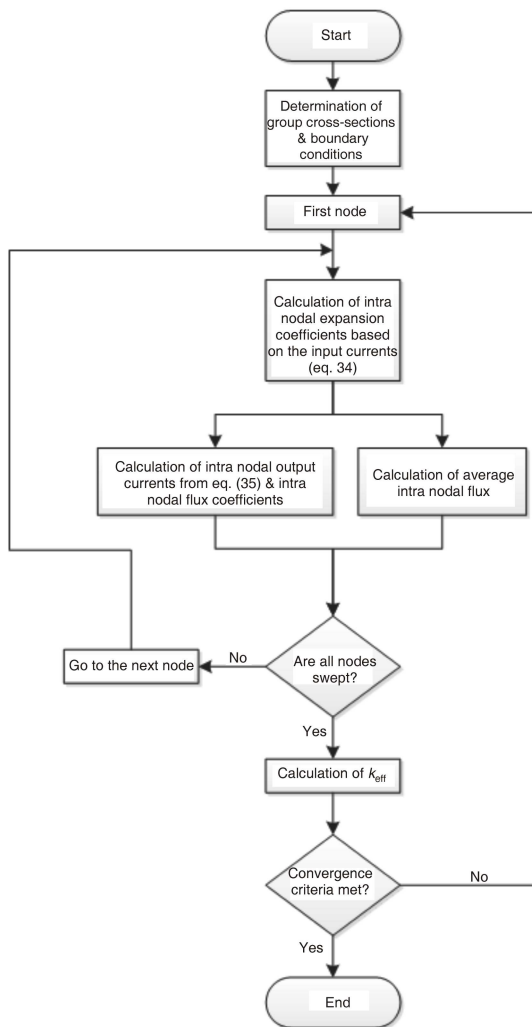


Figure 3. Flowchart of MA.CODE

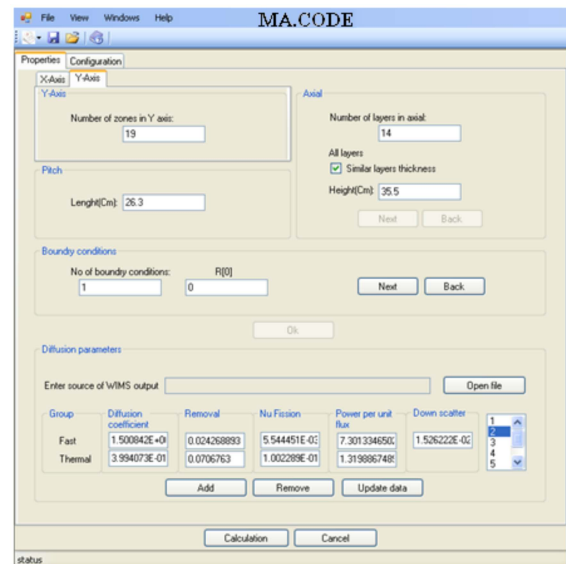


Figure 4. Main window of the MA.CODE

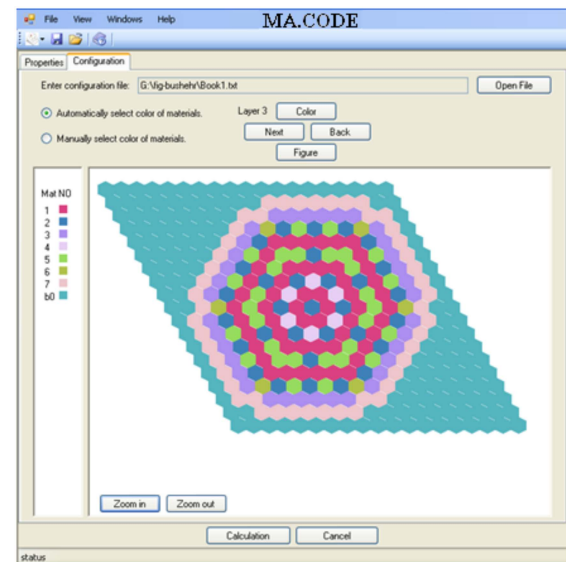


Figure 5. Core configuration in the MA.CODE

The whole procedure for the MA.CODE is sketched in the flowchart of fig. 3.

In a user friendly environment, the MA.CODE requires a number of nodes in the radial and axial directions, as well as the lattice pitch and boundary conditions for hexagonal nodes. The code is coupled with WIMS D5 and reads the cross-sections from WIMS automatically (see fig. 4).

The core configuration sketched in the MA.CODE can be seen in fig. 5.

## CONCLUSION AND DISCUSSION

In this paper we have used the FENM with the introduction of the volumetric average flux ( $\varphi_{total}$ ).

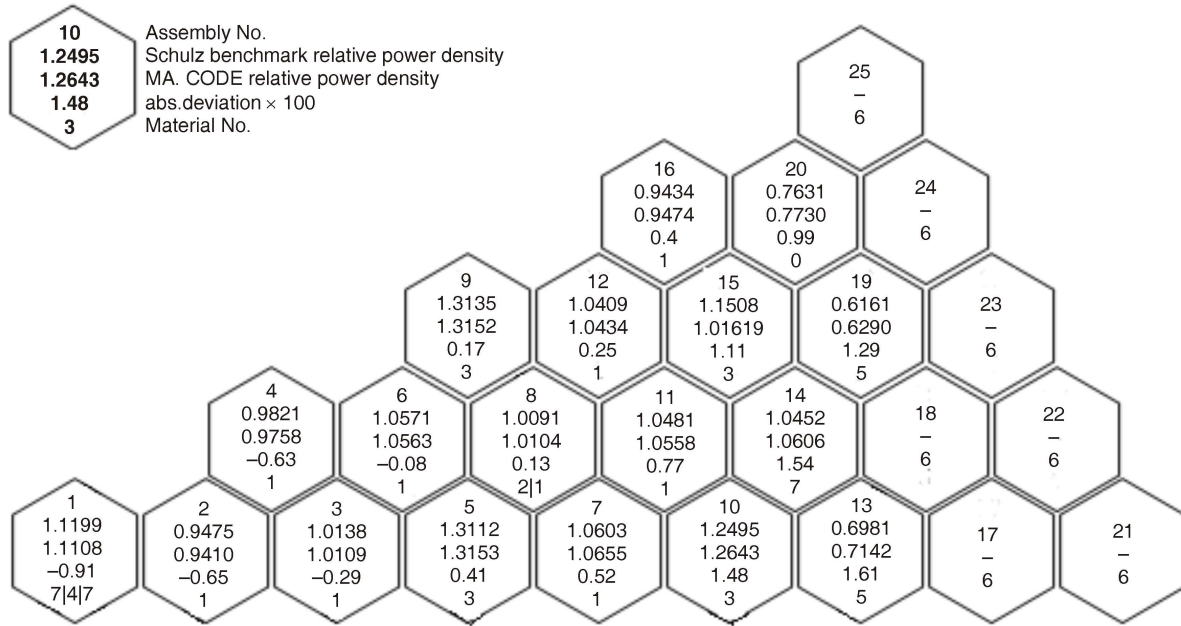


Figure 6. Comparison between MA.CODE results with AER-FCM-101 (Schulz) benchmark

Taking in consideration the external boundary conditions and the continuity of partial currents in the vicinity of nodal surfaces, we have calculated the flux coefficients for each node. By substituting the flux coefficients in the volumetric average flux correlation, the average neutron flux for each group and node is achieved. Thus,  $K_{eff}$  can be easily calculated from the Power-Method.

By the analytical solution of the integrals of flux and current on the surface of the hexagonal node with respect to fig. 1, fig. 2, and eqs. (19) to (29), using the symmetry of the hexagonal node and considering eq. (21), we have obtained significant results concerning the relation between the flux and current coefficients using the buckling mode. In two parallel node surfaces,  $A_m$  flux and current coefficients in  $\mu$ , ( $\lambda_m$  and  $\lambda_m$ ) are symmetric and  $B_m$  flux and current coefficients are equal, but in  $\mu$  this is reverse.

For the sake of benchmarking, we have compared the results from the flux expansion nodal method (FENM) using our code (MA.CODE) with two IAEA benchmarks, i. e. AER-FCM-101 [8], also known as the Schulz benchmark and AER-FCM-001 [9], known as Seidel's benchmark.

The FENM method proposed in this paper shows a good agreement with these two benchmarks. The effective multiplication factor for the Schulz benchmark was 1.04953, while our code calculates 1.049848 (i. e. 0.03% error). The comparison between MA.CODE fuel assembly relative power densities with the AER-FCM-101 benchmark is given in fig. 6. Relative power densities from the MA.CODE and AER-FCM-101 benchmark for fuel assembly no. 1 are also compared in fig. 7.

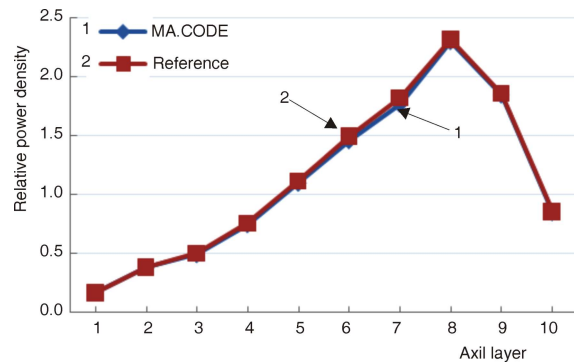


Figure 7. Comparison between relative power densities from MA.CODE with AER-FCM-101 (Schulz) benchmark for fuel assembly no. 1

The effective multiplication factor for Seidel's benchmark was 1.011470, while our code calculates 1.012104 (i. e. 0.06% error). The comparison between the MA.CODE fuel assembly relative power densities and the AER-FCM-001 benchmark is given in fig. 8. Relative power densities from the MA.CODE and AER-FCM-001 benchmark for fuel assembly no. 1 are also compared in fig. 9.

#### AUTHOR CONTRIBUTIONS

The theoretical analysis was carried out by M. Mohammadnia and A. Pazirandeh. Analytical solutions of the equations and C# programming computer code were carried out by M. Mohammadnia. The manuscript was prepared by all authors and the figures and tables by M. Mohammadnia and A. Pazirandeh.

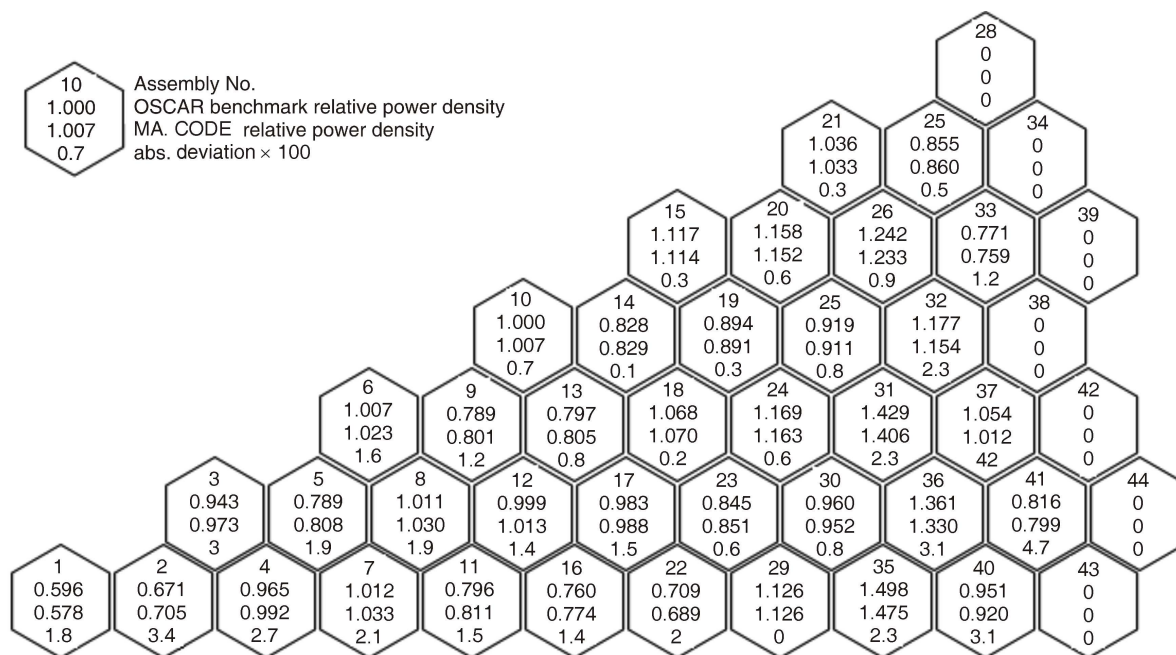


Figure 8. Comparison between MA.CODE results with AER-FCM-001 (Siedel's) benchmark (OSCAR)

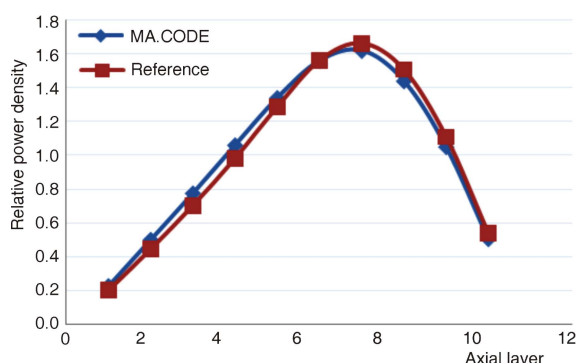


Figure 9. Comparison between relative power densities from MA.CODE with AER-FCM-001 (OSCAR) benchmark for fuel assembly no. 1

REFERENCES

[1] Stacey, W. M., Nuclear Reactor Physics, John Wiley & Sons Inc., New York, USA, 2007  
 [2] Cho, N. Z., Noh, J. M., Analytic Function Expansion Nodal Method for Hexagonal Geometry, *Nucl. Sci. Eng.*, 121 (1995), pp. 245-253  
 [3] Chao, Y. A., Shatilla, Y. A., Conformal Mapping and Hexagonal Nodal Methods – II: Implementation in the ANC-H Code, *Nucl. Sci. Eng.*, 121 (1995), pp. 210-225  
 [4] Noh, J. M., Cho, N. Z., ???, *Proceedings, International Conference on the Physics of Reactors (PHYSOR 96), Atomic Energy Society of Japan, 1* (1996), pp. A50-A59  
 [5] Chao, Y. A., Tsolfanidis, N., Conformal Mapping and Hexagonal Nodal Methods – I: Mathematical Foundation, *Nucl. Sci. Eng.*, 121 (1995), pp. 202-209  
 [6] Xia, B., Xie, Z., Flux Expansion Nodal Method for Solving Multi-Group Neutron Diffusion Equations in

Hexagonal-z Geometry, *Ann. Nucl. Energy*, 33 (2006), pp. 370-376  
 [7] Downar, T., Lee, D., Xu, Y., Kozlowski, T., Theory Manual for the PARCS Neutronic Core Simulator, PARCS, U.S. NRC, 2.6, 2004  
 [8] Schulz, G., Solutions of a 3-D VVER-1000 Benchmark, *Proceedings, 6<sup>th</sup> Symposium of AER on VVER Reactor Physics and Safety*, Kirkkonummi, Finland, 1996  
 [9] Seidel, F., Diffusion Calculations for VVER-440 2D and 3D Test Problem, *Proceedings, 14<sup>th</sup> Symp. of TIC*, 1, 1985, p. 216  
 [10] Pazirandeh, A., et al., Developing a Nuclear Neutronic Code in Rectangular, Triangular and Cylindrical Geometry, *Journal of Nuclear Science and Technology*, 63 (2013), pp. 44-53 ([www.aeoi.org.ir](http://www.aeoi.org.ir))  
 [11] Mohammadnia, M., et al., Design a Computational Program to Calculate the Composition Variations of Nuclear Materials in the Reactor Operations, *Annals of Nuclear Energy*, 57 (2013), pp. 111-113

Received on January 19, 2013  
 Accepted on August 23, 2013

**Мејсам МОХАМАДНИЈА, Али ПАЗИРАНДЕХ, Мостафа СЕДИГИ**

**РАЗВОЈ ПРОГРАМА ЗА НЕУТРОНСКЕ ПРОРАЧУНЕ ЈЕЗГРА  
НУКЛЕАРНОГ РЕАКТОРА СА ХЕКСАГОНАЛНОМ ЋЕЛИЈОМ  
МЕТОДОМ НОДАЛНОГ РАЗВОЈА ФЛУКСА**

Метода нодалног развоја флукса погодна је за разматрање ефекта нодализације у нодним угловима, а у овом раду коришћена је за аналитичко решавање међунодалног флукса. На овој основи развијен је рачунски програм под именом MA.CODE у програмском језику C#. Програм је оспособљен за прорачун реакторског језгра са хексагоналном геометријом ћелије, у две енергетске групе и три димензије. Програмом MA.CODE преузимају се двогрупне константе из програмског пакета WIMS и израчунавају ефективни фактор умножавања, флуксеви термалних и брзих неутрона у три димензије, густина снаге, реактивност и фактор пика снаге за сваки горивни ансамбл. Међу врлинама програма су брзина прорачуна и једноставан кориснички приступ. Резултати програма MA.CODE добро се слажу са IAEA тестовима, на пример, AER-FCM-101 и AER-FCM-001.

*Кључне речи: нодална метода, хексагонална геометрија, расподела неутронског флукса, MA.CODE*

---